Atmos. Chem. Phys. Discuss., 10, 16691–16745, 2010
www.atmos-chem-phys-discuss.net/10/16691/2010/
doi:10.5194/acpd-10-16691-2010

Atmospheric Chemistry and Physics Discussions

Modeling of photolysis rates over Europe: impact on chemical gaseous species and aerosols

E. Real and K. Sartelet

CEREA, ENPC/EDF, 20 rue Alfred Nobel 77455 – Champs sur Marne, France

Received: 13 April 2010 – Accepted: 29 May 2010 – Published: 5 July 2010

Correspondence to: E. Real (elsa.real@cerea.enpc.fr)

Published by Copernicus Publications on behalf of the European Geosciences Union.

Abstract

This paper evaluates the impact of photolysis rate calculation on European air composition and air quality monitoring. In particular, the impact of cloud parametrisation and the impact of aerosols on photolysis rates are analysed. Photolysis rates are simulated using the Fast-JX photolysis scheme and gas and aerosol concentrations over Europe are simulated with the regional model Polair3D of the Polyphemus platform. The photolysis scheme is first use to update the clear sky tabulation used in the previous Polair3D version. Important differences in photolysis rates are simulated, mainly due to updated cross-sections in the Fast-JX scheme. In the previous Polair3D version, clouds were taken into account by multiplying the clear-sky photolysis rates using a correction factor. In a second stage, the impact of clouds is taken into account more accurately by simulating them directly in the photolysis scheme. Differences in photolysis rates inside clouds are as high as differences between simulations with and without clouds. Outside clouds, the differences are small. The largest difference in gas concentrations is simulated for OH with a mean increase of its tropospheric burden of 4 to 5%.

To take into account the impact of aerosols on photolysis rates, Polair3D and Fast-JX are coupled. Photolysis rates are updated every hour. Large impact on photolysis rates is observed at the ground, decreasing with altitude. The aerosol species that impact the most photolysis rates is dust especially in South Europe. Strong impact is also observed over anthropogenic emission regions (Paris, The Po and the Ruhr Valley) where mainly nitrate and sulphate reduced the incoming radiation. Differences in photolysis rates lead to changes in gas concentrations, with the largest impact simulated for OH and NO concentrations. At the ground, monthly mean concentrations of both species are reduced over Europe by around 10 to 14% and their tropospheric burden by around 10%. The decrease in OH leads to an increase of the life-time of several species such as VOC. For example, isoprene ground concentrations increase in average by around 10%. NO_2 concentrations are not strongly impacted and O_3 concentrations are mostly

ACPD

10, 16691–16745, 2010

reduced at the ground with a monthly mean decrease of about 3%. O_3 peaks are systematically decreased because of the NO_2 photolysis rate decrease. Not only gas are impacted but also secondary aerosols, due to changes in gas precursors concentrations. Monthly mean concentrations of nitrate, ammonium, sulphate and secondary organic aerosol at the ground are modified by up to 4% but PM_{10} and $PM_{2.5}$ only by 1 to 2%. However monthly mean local differences in PM_{10} and $PM_{2.5}$ concentrations can reach 8% over regions with strong production of secondary aerosols such as the Po valley.

In terms of air quality monitoring, ground concentrations of O_3, NO_2 and PM_{10} are compared with measurements from the EMEP stations. Statistics are usually better for simulation taking into account aerosol impact on photolysis rates, but changes are small. On the other hand, the systematic O_3 peak reduction leads to large differences in the exceedances of the European O_3 threshold as calculated by the model. The number of exceedances of the information and the alert threshold is divided by 2 when the aerosol impact on photochemistry is simulated. This shows the importance of taking into account aerosols impact on photolysis rates in air quality studies.

1 Introduction

Photolysis reactions play a major role in the atmospheric composition. In the troposphere, they drive both O_3 production through NO_2 photolysis (λ<330 nm):

$$NO_2 + h\nu \xrightarrow{JNO_2} NO + O(^3P)$$
$$O(^3P) + O_2 + M \longrightarrow O_3 + M$$

and O_3 destruction through its own photolysis (λ<420 nm) :

$$O_3 + h\nu \xrightarrow{JO_3} O_1D + O_2$$

ACPD
10, 16691–16745, 2010

This latest reaction is also the main source of OH radicals (in presence of water vapour):

$$O_2 + H_2O \longrightarrow 2OH \quad (1)$$

OH radical is the primary oxidising sink of CO, methane and other hydrocarbons. It also drives the formation of oxidised forms of nitrogen species (PAN and HNO_3) and therefore the availability of NO_2 for O_3 formation.

Furthermore OH is involved in the formation of secondary aerosols as the main oxidant of their gas precursors: SO_2 for the formation of sulphate, VOC (Volatile Organic Hydrocarbons) for the formation of Secondary Organic Aerosol (SOA) and NO_2 for the formation of HNO_3 which may condense to form nitrate.

Because of their impacts on both gas and aerosol atmospheric compositions, photolysis rates need to be accurately modeled in global tropospheric studies and regional air quality studies.

The photolysis rates $J(i)$ for a gaseous species i depend on the wavelength λ and can be described as follow:

$$J(i) = \int_{\lambda} \sigma_i(\lambda,P,T)\Phi_i(\lambda,P,T)F(\lambda)d\lambda \quad (2)$$

where σ_i and Φ_i are, respectively the absorption cross section and the quantum yield of the i species, and F is the actinic flux representative of the irradiance that reaches the level where J is calculated. σ_i and Φ_i are specific to the photolysed species i whereas F depends on the position of the sun but also on the presence of clouds and aerosols. To correctly simulate photolysis rates, it is necessary to precisely know the absorption cross sections and the actinic flux. The largest incertitude on the actinic flux is the impact of clouds and aerosols.

In an aerosol layer, light beams can be either scattered or absorbed depending on the aerosol optical characteristic, i.e. their Optical Properties (OP) at the beam wavelength, and their Optical Depth (OD) which, given their OP, characterised the aerosol

ACPD
10, 16691–16745, 2010

loading. In a cloud layer, light is only scattered. Impact on photolysis rates of aerosols and clouds is important in the layer but also below and above it.

In global chemistry atmospheric models, the alteration of solar radiation by aerosols is often directly taken into account by calculating on-line photolysis rates, i.e. by calculating photolysis rates directly in the chemistry atmosphere model (Martin et al., 2003; Tie et al., 2005). However this impact is most of the time ignored in air quality studies at the regional scale. To our knowledge, there is only one study performed with a regional model that reports the regional impact of modifications of photolysis rates by aerosols on gas concentrations in Asia (Tang et al., 2003). The large majority of air quality models or regional CTMs do not calculate on-line photolysis rates and only use a pre-calculated tabulation of clear-sky photolysis rates. The tabulation depends on the latitude, the time of the year and the SZA. Aerosols are usually taken into account as a spatially and temporally uniform attenuation factor when computing the clear-sky tabulated photolysis rates. To model the attenuation of solar radiation by clouds, the clear-sky tabulated photolysis rates are usually multiplied by an attenuation coefficient which depends on cloud model data.

Several global model studies analysed the impact on gas concentrations of taking into account the alteration of solar radiation by aerosols (Liao et al., 2003; Martin et al., 2003; Tie et al., 2005). Results were inhomogeneous but all studies simulated a decrease of photolysis rates at the ground. The highest decrease of monthly mean photolysis rates was simulated below dust and forest fire aerosols (up to −50% in Martin et al., 2003) which are both absorbing species. Impact on gas concentrations was strong for global OH tropospheric burden but not really for global O_3 burden. However, strong regional impact was simulated (up to −5 to −15% of ground O_3 concentrations over biomass burning regions). The impact on aerosol concentrations has not been studied yet.

In this study, the impact of the alteration of photolysis rates by clouds and aerosols is studied at a regional scale over Europe. Not only the modifications of photolysis rates are analysed but also those of gas concentrations and the formation of secondary

ACPD
10, 16691–16745, 2010

aerosols. Even though vertical profiles are discussed, emphasis is given on impact on ground concentrations and regional air quality. At first, the regional CTM is briefly discussed, as well as the photolysis scheme used and the online treatment of solar-radiation alteration by clouds and aerosols. In the second part, the impact of using two different photolysis scheme on clear-sky photolysis rates is studied. The impact of the parametrisation used for modeling the alteration of solar radiation by clouds and the aerosol impact on solar radiation are then detailed. Finally, the impact on air quality monitoring is studied. The objective of this paper is to estimate how a more realistic simulation of photolysis rates influences air quality and regional air composition.

2 Model description and setting of the simulation

2.1 Model description

2.1.1 The Chemistry Transport Model: Polair3D of the Polyphemus platform

Polyphemus is a platform containing several atmospheric models (Gaussian, Eulerian, Lagrangian). The Chemistry Transport Model (CTM) Polair3D of Polyphemus has been used for many applications: e.g. sensitivity analysis of ozone (Mallet, 2005), of particulate matter (Sartelet et al., 2007a), modeling of mercury and heavy metal at continental scale (Roustan and Bocquet, 2006), data assimilation (Krysta et al., 2006) etc. . . . The simulations presented here are carried out at a continental scale, over Europe for 2 months (July and November 2001). The model has been validated for the year 2001 over Europe (Sartelet et al., 2007a) with respect to 3 European databases (European Monitoring and Evaluation Programme (EMEP), BDQA and AirBase). It has also been used over Asia (Carmichael et al., 2008) or Greater Tokyo (Sartelet et al., 2007b).

For gaseous chemistry, the chemical mechanism used in the model is the Regional Atmospheric Chemistry Mechanism (RACM) (Stockwell et al., 1997) (82 gas species). Aerosols are simulated using the SIze REsolved Aerosol Model (SIREAM) (Debry

ACPD
10, 16691–16745, 2010

et al., 2007). SIREAM includes 16 aerosol species: 3 primary (mineral dust, black carbon and primary organic species), 5 inorganic species (ammonium, sulphate, nitrate, chloride and sodium) and 8 organic species modeled by the Secondary ORGanic Aerosol Model (SORGAM) (Schell et al., 2001). The thermodynamic module used for inorganics is ISORROPIA (Nenes et al., 1998).

Aerosols and gas are scavenged by dry deposition, below-cloud scavenging and in-cloud scavenging. Coagulation and condensation are taken into account and gas and aerosols are assumed to be in thermodynamic equilibrium. Aqueous-phase chemistry inside droplets is modeled with the Variable Size Resolved Model (Fahey and Pandis, 2003).

In the standard version of Polyphemus, photolysis rates are extracted from a clear-sky tabulation. In previous simulation with the model Polair3D, the tabulation is computed with the JPROC photolysis scheme, based on a delta-Eddington two-stream radiative model (Joseph et al., 1976). Aerosol impact on photolysis rates is taken into account in a very simple way: a constant tropospheric aerosol profile with an optical depth of 0.3 is assumed all over the globe. Modification of photolysis rates by clouds is accounted for by using an attenuation coefficient (see Sect. 2.1.3). In this paper, both cloud and aerosol impact on photolysis rates are simulated in a more realistic way using the photolysis scheme Fast-J.

Detail set-up of the version of Polair3D used for this study is described Sect. 2.2.

2.1.2 The photolysis scheme: Fast-J

Fast-J is a photolysis scheme designed to be used on-line in CTM (Wild and Akimoto, 2001). It computes photolysis rates taking into account the multiple-scattering in the UV and visible parts of the spectrum, in, above and below clouds and aerosols. Fast-J solves the multiple-scattering behaviour by using an accurate numerical solution based on Legendre expansion of the scattering phase function, which is the parameter describing the 3-D scattering comportment of aerosols (Wild and Akimoto, 2001). As the Legendre expansion is cut at its 8th terms, the solution is called “8-stream multiple

ACPD
10, 16691–16745, 2010

scattering solution". In J-PROC, the scattering function is only described by one parameter giving information on the forward versus the backward scattering: a two-stream approach. Fast-J uses 18 wavelength bins to discretise the solar spectrum. This is much less than other radiative models (usually more than 170 as in JPROC) in order to save computational time. Aerosols and clouds are represented in the model through their optical depth and optical properties at different wavelengths. Fast-J requires the following OP as input of the model: the single scattering albedo, the extinction coefficient and the phase function (expressed as the 8 first terms of its Legendre expansion). These OP are usually calculated with a Mie model and depend on the aerosol refractive index and aerosol size or on the droplet size (or ice crystals size) for the cloud. Pre-calculated values of OP are included in Fast-J for several cloud droplet sizes and ice crystal shapes.

In this paper, the last updated version of Fast-J, namely Fast-JX is used. Photolysis rates calculated by the Fast-J model have been evaluated both at the surface (Barnard et al., 2004) and through the troposphere in the presence of clouds (Voulgarakis et al., 2009). Firstly, a clear-sky tabulation is computed and compared with the old tabulation computed with JPROC (Sect. 3.1). Then, instead of using the Fast-JX clear-sky tabulation along with an attenuation coefficient for clouds, on-line treatment of clouds in the photolysis scheme Fast-JX is performed and both methods are compared (Sect. 3.2). Finally, the aerosol impacts on photolysis rates are taken into account by coupling Fast-JX and Polair3D (on-line photolysis calculation) (Sect. 3.3).

2.1.3 On-line treatment of the solar radiation alteration by clouds

In the standard version of Polyphemus, the impact of clouds on photolysis rates is calculated through an attenuation coefficient A_{tt} applied to clear-sky photolysis rates (Mallet, 2005). In this parametrisation, similar to the technique used by Chang et al. (1987), clouds are represented as a single layer. Then, the attenuation coefficient depends on the Solar Zenith Angle (SZA), the Liquid Water Content (LWC) and whether the level considered is above, in or below the single cloud layer.

ACPD
10, 16691–16745, 2010

This parametrisation can be seen as a first-order approach but there is some conditions under which the approximation is inappropriate, for example in the presence of multiple layers of clouds or for a deep cloud where attenuation is strongly non-linear (Wild et al., 2000). In such case, a photolysis scheme that directly calculates photolysis rates in the presence of clouds is necessary. Here the Fast-J model is used. Cloud OD τ is computed in each layer of the model if a cloud is diagnosed (Cloud Fraction>0). There exists several studies based on experimental, field or satellite data to estimate cloud OD from the LWC. In this study we used the formula of Rockel et al. (1991) adapted by Pozzoli et al. (2008) to calculate the OD τ from both the LWC and the IWC (Ice Water Content):

$$\tau = a_{\mathrm{w},\lambda} \times \mathrm{LWP} \times r_{\mathrm{eff,w}}^{b_{\mathrm{w},\lambda}}$$

$$\tau = a_{\mathrm{i},\lambda} \times \mathrm{IWP} \times r_{\mathrm{eff,i}}^{b_{\mathrm{i},\lambda}}$$

where LWP and IWP represent the liquid and ice water paths, i.e. the integration of the LWC and the IWC over the altitude. The parameters $a_{\mathrm{w},\lambda}$, $b_{\mathrm{w},\lambda}$ (for water) and $a_{\mathrm{i},\lambda}$, $b_{\mathrm{i},\lambda}$ (for ice) were derived from the Rockel et al. (1991) results. Those results were fitting at the wavelengths used in Fast-JX by Pozzoli et al. (2008) resulting in the following values: $a_{\mathrm{w},\lambda}$=1.488, $b_{\mathrm{w},\lambda}$=−0.9374, $a_{\mathrm{i},\lambda}$=1.911 and $b_{\mathrm{i},\lambda}$=−1.0631. The droplet and ice crystal effective radius, $r_{\mathrm{eff,w}}$ and $r_{\mathrm{eff,i}}$, are prescribed (10 µm and 50 µm, respectively) and different values are tested (Sect. 3.2).

Appart from OD, the other parameters required by Fast-JX are the cloud OP i.e. the single scattering albedo, the extinction coefficient and the phase function. Here, we use the Fast-JX prescribed values (see Sect. 2.1.2). They mainly depend on the droplet size (for water cloud) and ice crystal shape (for ice cloud). Different size of droplets are tested (Sect. 3.2) with a default value of 10 µm. By default, ice clouds with irregular ice crystals are used. Sensibility study on the presence of ice is conducted in Sect. 3.2.

Specification of cloud OD, OP and cloud fraction in each layer are not sufficient to calculate radiative transfer. In general clouds do not cover the entire horizontal grid box

ACPD
10, 16691–16745, 2010

of the model (this is represented in the meteorological model by cloud cover fraction data). Knowledge of how multiple cloud layers overlap, i.e. knowledge of the cloud vertical coherence, is therefore required to calculate cloud OD.

Several complex schemes have been developed to take into account this cloud overlapping, mainly in global climate models (Wang and Rossow, 1998; Collins, 2001) but also in global CTMs (Feng et al., 2004; Neu et al., 2007). One of the most famous scheme is called the max/random overlap scheme but is computationally expensive because it requires random calculation of the cloud vertical coherence (Geleyn and Hollingsworth, 1992). A good approximation of the max/random overlap scheme has been developed by Briegleb (1992) and used in CTM studies (Feng et al., 2004; Pozzoli et al., 2008). In this scheme, the cloud OD in each layer is weighted by the cloud cover fraction raised to the power of 3/2. This overlap scheme is chosen for this study.

2.1.4 On-line treatment of the solar radiation alteration by aerosols

Photolysis rates in the presence of clouds can be computed in a preprocessing stage (i.e. before running the CTM) as only meteorological data (relative humidity, LWC and IWC data) are required to run the photolysis scheme. In contrast, photolysis rate calculation in the presence of aerosols must be done on-line in the CTM, as aerosol concentration fields are calculated at each model time-step.

In the on-line treatment of the aerosol impact on solar radiation, OD and OP are calculated at each grid box of the CTM from the simulated aerosol 3-D concentrations. The OD and OP 3-D distributions are then used as input of the photolysis scheme Fast-JX which calculates photolysis rate 3-D distribution. Newly calculated photolysis rates are used for the next time step of the CTM to calculate gas and aerosols concentrations. Thereby, the simulated aerosol concentrations influence the photolysis rates, which directly influence the gas-phase concentrations. The impact on gas-phase concentrations also induces an impact on aerosol concentrations.

To translate aerosol concentrations in OD (vertical integration of the extinction coefficient) and OP (single scattering albedo, extinction coefficient and phase function),

ACPD
10, 16691–16745, 2010

the method used by Tombette et al. (2008) is used: given the particle refractive index and its wet diameter, a tabulation based on a Mie code (called Mie table) provide the OP. The Mie model developed by Mishchenko et al. (1999) is used here because it calculates the 8 first terms of the Legendre expansion of the phase function (see Sect. 2.1.2), required by Fast-J.

The refractive index of a particle composed of several species can be estimated from the individual refractive indexes of each aerosol species, with assumptions on the particle mixing state. Here, refractive indexes of all individual aerosol species are taken from the OPAC (Optical Properties of Aerosols and Clouds; Hess et al., 1998) software package. All aerosol species are assumed to be well mixed except black carbon that constitutes a core. The wet diameter is calculated using the aerosol liquid water content calculated in the CTM with Isoropia.

In this study, photolysis rates are updated (re-calculated with Fast-JX from aerosol concentrations) every hour and are then considered as constant. For the simulation described below, the computing time is only increased by 2.5% when using a frequency of update of 1 h. Simulations with photolysis rate updated every hour and every 10 min have been compared and only very small differences in the gas and aerosol concentrations (<1%) were found.

2.2 Model set-up

The model was run for the months of July and November 2001 over Europe. Model set-up is the same as in Sartelet et al. (2007a) except for the vertical resolution. The main characteristics of the configuration are summarized below.

The horizontal step is $0.5^{\circ}\times0.5^{\circ}$ and 13 vertical levels from 0 to 10 km are used. Meteorological fields are provided by the European Centre for Medium-range Weather Forecast with an horizontal step of $0.36^{\circ}\times0.36^{\circ}$ and a 3 h time-step. The boundary conditions for gas are taken from the MOZART 2 model (Horowitz et al., 2003) and from the GOCART model (Chin et al., 2000) for aerosol concentrations. In previous studies, GOCART dust boundary conditions were reduced by 4 (Vautard et al., 2005;

ACPD
10, 16691–16745, 2010

Sartelet et al., 2007a). To validate this drastic division, the GOCART simulated total optical depth was compared to measurements from the AERONET (AErosol RObotic NETwork) database for the entire year 2001 over Europe. The GOCART simulated ODs were too high. However, when dividing the GOCART dust concentrations by 4, all statistics (see appendix for a definition of the different statistics) were strongly improved for the months of July and November (see Table 2).

3 Results and discussion

As explained in Sect. 1, the two photolysis rates JNO_2 and JO^1D, are very important to understand tropospheric chemistry as they influence, respectively O_3 production and O_3 destruction, as well as OH production. In the following section, when analysing impact on photolysis rate, we mainly focus on these 2 photolysis rates, even though others photolysis rates are mentioned. Induced impact on gas and aerosol concentrations are also analysed both in the whole troposphere and at the ground level.

Differences between simulations are mainly expressed in terms of relative differences. When not specified these relative differences are calculated at each grid point of the model (local relative differences) and each time-step. Then they are averaged over the simulated month.

3.1 Impact of changing the photolysis scheme

In this section, we briefly study the sensitivity of photolysis rates and concentrations on the photolysis scheme. Two photolysis schemes used to compute clear-sky tabulation of photolysis rates are compared. This is interesting in order to understand what parameters, data or physical hypothesis influence most the photolysis rate calculation and what changes are expected when changing or updating the photolysis scheme used in a CTM.

ACPD
10, 16691–16745, 2010

The main differences between the two photolysis schemes in their default configuration (JPROC and FAST-JX) are summarised in Table 3. The two models used different physical treatment of scattering, number of wavelength bins, O_3 profiles, temperature, O_2 and aerosol profiles as well as different earth albedo and cross-sections. In JPROC, cross sections from RADM dated from 1988 are used whereas updated JPL 2002 cross-sections (Sander et al., 2002) are used in Fast-JX. With these configurations, important differences are found between photolysis rates simulated with these two different tables. For the photolysis rates of NO_2 and O_3, mean relative differences of 21 and 32% are simulated. Differences can be much larger for some photolysis rates, as for example HNO_3 (63%) or HNO_4 (219%).

Different tests have been conducted to understand which parameters drive the differences in photolysis rates between the 2 models. We found that when using the same aerosol profiles, the same earth albedo and the same cross-sections for both models, differences in photolysis rates are reduced to values between 1 and 12% (for all photolysis rates). Among the 3 parameters identified as the most influencing the photolysis rates, differences in cross-sections dominate (on average, about 70% of the photolysis differences are due to cross-section differences). Aerosol profiles and earth albedo both account for around 10%. The remaining differences probably come from the intrinsic use of 18 wavelengths in Fast-JX instead of 171 in JPROC, which should be lower than 3% according to Wild and Akimoto (2001), and from the intrinsic difference in scattering treatments in both models (2 streams against 8 streams).

CTM simulated concentrations with both photolysis schemes also show important differences. We will not details results in this paper but mean tropospheric OH, O_3 and NO differences of 26, 1, 20% and 14, 3 and 16%, respectively in winter and summer are found.

To resume, large differences on photolysis rates are found when using the 2 different photolysis schemes (Fast-JX and JPROC) to compute clear-sky photolysis rates, leading to large differences in gas concentrations calculated by the CTM. These differences are mainly due (around 70%) to differences in cross-sections data. Intrinsic differences

ACPD
10, 16691–16745, 2010

between the models (i.e. wavelength bins and scattering treatments) do not account for more than 12% of the differences. This comparison underlines the importance of using updated cross-sections when computing photolysis rates.

3.2 Impact of the parametrisation used for modeling alteration of solar radiation by clouds

In this section we compare photolysis rates and gas concentrations calculated with the "attenuation" method (clear-sky tabulated photolysis calculated with Fast-JX multiplied by an attenuation factor), to those calculated with the photolysis scheme Fast-JX in presence of clouds, namely the "cloud on-line" method.

3.2.1 Impact on photolysis rates

Photolysis rates are calculated for the months of November and July 2001, with clear-sky conditions (R-CSKY) and with the "attenuation" (R-ATT) and "cloud on-line" (R-COnL) parametrisations.

Mean vertical O_3 and NO_2 photolysis rate profiles are shown in Fig. 1 for the R-CSKY, R-ATT and R-COnL cases. The mean cloud OD calculated for each month is also shown in this figure. In average, the R-COnL photolysis rates are higher than the R-ATT ones. The largest differences between R-ATT and R-COnL are located inside clouds (between 1 and 3 km in winter and 1 and 5 km in summer) and slightly above, especially in winter. At these vertical levels, the differences between the 2 cloud simulations R-ATT and R-COnL (around 10%) are of the same order of magnitude than differences between R-ATT and a simulation without clouds. The maximum daily relative differences between R-ATT and R-COnL photolysis rates (not shown) is around 40%. It is found in clouds, usually correlated with high cloud OD. Below clouds, differences are much lower, not higher than a few percent on average.

Although in average both JNO_2 and JO^1D are higher with on-line cloud calculation (R-COnl) than with the attenuation parametrisation (R-ATT), R-COnl JNO_2 are slightly lower below clouds in winter as well as R-COnl JO_3 above clouds in summer. The

ACPD
10, 16691–16745, 2010

variations of JNO_2 and JO^1D are not everywhere the same sign (positive or negative) because these photolysis rates are influenced by radiations of different wavelengths.

The same kind of features (higher photolysis rates when clouds are simulated on-line in the photolysis scheme, with some rare exceptions) are observed in Wild et al. (2000). In this study, on-line calculation with the same Fast-J photolysis scheme embedded in a global CTM model is compared with the Chang et al. (1987) technique (equivalent to our R-ATT run). They showed that differences in and above clouds are particularly important in deep clouds and in presence of several vertical cloud layers. In those cases the benefit of the full scattering calculation performed in Fast-J is clear.

In order to evaluate the sensitivity of the results to the size of the droplets (used in the calculation of the cloud OD and OP) and the presence of ice, sensitivity tests were conducted with droplets of 3 and 20 µm (instead of 10 µm) and with no ice in clouds. Mean differences (not shown) are very small (not higher than 2%) suggesting that the droplet size and ice shape do not strongly influence the photolysis rates It is not surprising that the presence or absence of ice do not change photolysis rates much because the ice cloud OD is only about 5% of the water cloud OD (mainly due to the low ice water content in ECMWF data).

3.2.2 Impact on 3-D concentrations

Monthly mean vertical profiles of relative differences between species simulated with R-COnL and R-ATT are represented in Fig. 2 for O_3, OH, NO and NO_2.

OH concentrations respond directly to changes in O_3 loss ($O_3+h\nu \rightarrow O^1D+O_2$ leads to OH formation in the presence of water vapor). It depends on O_3 photolysis rate values but also on O_3 concentrations. In general OH concentrations change with O_3 photolysis changes. One exception is found in winter close to the ground. In this case, the O_3 photolysis rate slightly increases but OH concentrations decrease. This can be explained by the decrease in O_3 concentrations that compensates for the photolysis rate increase.

ACPD
10, 16691–16745, 2010

Increase in NO_2 photolysis rate generally leads to a decrease in NO_2 concentrations and an increase in NO concentrations. One noticeable exception is found in the boundary layer in summer where a mean decrease in NO is simulated with a mean increase in NO_2 photolysis. This is related to diurnal variations of photolysis rates and NO concentrations in the boundary layer. Further explanations for this feature are given on the next section.

The behaviour of O_3 is more complex. An increase in the NO_2 photolysis rate leads to an increase in O_3 production whereas increase in the O_3 photolysis rate destroys O_3. An increase in photolysis rates can therefore lead to O_3 net production or destruction. If air masses are in a net O_3 production regime (O_3 production>O_3 destruction), a similar increase (respectively decrease) in O_3 and NO_2 photolysis rates will quantitatively increase (respectively decrease) more O_3 production than destruction, leading to an increase (respectively decrease) in O_3 net production. Similarly, if air masses are in a net destruction regime, an increase (decrease) in photolysis rates will lead to a decrease (increase) in O_3 concentrations. Because of this duality, differences will only be large where one of the two terms (O_3 production or destruction) strongly dominates the other. This explains why changes in O_3 are mainly simulated at the ground, where net O_3 production or destruction can be large, and not in the mean free troposphere where production usually compensates destruction.

Close to the ground, O_3 increases in summer and decreases in winter. In summer both JNO_2 and JO^1D increase and as air masses are generally in an O_3 production regime, this leads to a net O_3 increase. In winter, JNO_2 slightly decreases at the ground leading to a decrease in O_3 production together with an increase in JO^1D that increases O_3 loss. This explains the simulated net decrease of O_3.

Both in winter and summer, NO and OH are the most sensitive species to changes in photolysis rates because they are both short-life species. The largest changes are observed inside clouds (between 1 and 5 km) where the changes in photolysis rates are the most important (see previous section). These changes are more important in average in winter than in summer due to larger differences in photolysis rates induced

ACPD
10, 16691–16745, 2010

by the higher presence of clouds in winter (higher OD). Inside clouds in winter, relative differences of, respectively +15%, −4% and +10% are simulated for OH, NO_2 and NO. O_3 relative differences are maximum at the ground but less than 1% in average over Europe.

The relative differences in tropospheric burden are also calculated (see Table 3). In contrast to other "locale" relative differences calculated in this paper, these differences are not calculated locally but concentrations are first averaged over the domain (horizontal, temporal and vertical) for each of the 2 runs and then the difference is computed. This mean that important local changes on small concentrations do not strongly impact the tropospheric burden relative differences. Mean tropospheric burden changes simulated in winter are less than 1% for NO_2 and O_3 and about 2 and 5% for NO and OH whereas in summer they do not exceed 1% for NO and O_3 and are about 2.5% for NO_2 and 3% for OH.

3.2.3 Impact on ground concentrations

Only small impacts on ground concentrations are simulated with on-line clouds in Fast-JX. Local relative differences stay below 5% with the largest impact on OH concentrations and ground-burden differences remain below 1%.

As observed in the previous paragraph, NO concentrations computed with R-COnL are higher than with R-Att (see Fig. 2). However because monthly averaged NO_2 photolysis rate increases, we could think that NO_2 would decrease and NO increase. To understand this feature, daily variations of the NO_2 photolysis rate and NO concentrations are shown in Fig. 3. It can be seen that although the NO_2 photolysis rate decreases around noon, it increases at sun-rise and sunset. Scattering by particles depends on the light incidence angle. The smallest this angle, the more asymmetric the diffusion is (mainly forward diffusion). In Fast-J, the phase function which represents this asymmetry is well defined (to the 8th order). In the R-ATT simulation, this dependence is simulated through a simpler dependence on Solar Zenith Angle (SZA). This explains the differences in the photolysis rate variations simulated with R-COnL

ACPD
10, 16691–16745, 2010

and R-ATT with the SZA, and especially near sun-rise and sunset. NO concentrations show a peak in the morning, mainly due to emissions (morning traffic). Therefore, the morning increase of JNO_2 leads to a stronger quantitative decrease of NO than the increase of NO (due to JNO_2 decrease) around noon. This explains the decrease of daily NO concentrations.

Mean ground OH relative differences against mean cloud OD, averaged over the spatial domain and represented for each day are plotted in Fig. 4. There is a clear linear dependence of ground OH relative differences with the cloud OD. This traduces the fact that differences coming from the on-line representation of clouds in the photolysis rate scheme are particularly important for deep clouds as shown by Wild et al. (2000).

3.3 Aerosol impact on solar radiation

In this section the influence of aerosols on photochemistry through the alteration of photolysis rates is evaluated. To do so, the simulation R-COnL where only clouds are taken into account in the photolysis scheme, is compared to the simulation R-AERO where both clouds and aerosol concentrations impact photolysis rates. As previously, simulations are conducted for July and November 2001.

3.3.1 Impact on photolysis rates

We first briefly describe the simulated tropospheric Aerosol OD (AOD). Monthly mean spatial values of the AOD for the month of July are represented over Europe in Fig. 5 together with vertical AOD profile. Contributions to AOD from each aerosol type is also shown in the vertical AOD profile. The largest tropospheric AOD values are simulated over South Europe, due to dust aerosols coming from Africa, despite the reduction by a factor 4 of dust aerosols in the boundary conditions (see Sect. 2.2). Regions with strong anthropogenic emissions, such as Paris, the Po valley and the Ruhr valley also clearly contribute to the tropospheric AOD. In such regions, the component that contributes the most to the AOD is nitrate. Eastern Europe also contributes to AOD mainly

ACPD
10, 16691–16745, 2010

through sulphate (presence of power plant releasing large SO_2 concentrations) and to a lesser extent organic aerosols and black carbon. Overall, the component which impacts the most the AOD is dust followed by sulphate and nitrate. Dust is mainly present above the boundary layer (peak around 4 km) whereas other components exhibit peaks in the boundary layer (around 500 m). It should be noticed that forest fires are not included in the emissions. Black carbon concentrations may strongly influence AOD in case of biomass burning.

Mean vertical profiles (averaged over the spatial domain and over the month) of NO_2 and O_3 photolysis rates simulated with R-AERO in July and November 2001 are represented in Fig. 1.

Comparisons of the R-COnL and R-AERO simulations in Fig. 1 show that including the aerosol impact on solar radiation leads to a mean decrease of all photolysis rates (here only NO_2 and O_3 photolysis rates are shown) from the ground to 10 km, the highest vertical level simulated in our run. This decrease is strongest at ground level and decreases with altitude. He and Carmichael (1999) studied the effect on photolysis rates of an aerosol layer located in the boundary layer depending on aerosol types. They showed that for absorbing aerosols (like urban but also dust aerosols), photolysis rates were reduced through all the tropospheric column whereas for purely scattering aerosols the effect is mainly an increase of photolysis rates above the layer and different effects in and below the layer, depending on the aerosol numbers. In our case, the mean AOD is dominated by dust aerosols over the troposphere , which are partly absorbing. This explains that mean photolysis rates at all vertical levels are reduced. However, the impact of aerosols on photolysis rates is spatially heterogeneous. Figure 6 shows the monthly mean relative differences of JNO_2 at the ground in July. It can be seen that strong decreases of JNO_2 for the R-AERO run are correlated with high tropospheric AOD. JO^1D and other photolysis rates exhibit the same feature (not shown) with decrease of the same order of magnitude. At higher vertical levels (starting from around 500 m height), some regions with high concentrations of scattering aerosols (sulphate for example) in the lower vertical layers show positive differences

ACPD
10, 16691–16745, 2010

(largest photolysis rates when including aerosols) above these layers. This is the case for example over Paris, the Po Valley and the Ruhr valley (not shown).

On averaged (over the spatial domain) monthly mean JNO_2 and JO^1D decrease at the ground by, respectively 8 and 6.5% (with local maximum of 30% in South Europe) in summer and by 20 and 12% in winter. The decrease is more important in winter because SZA are larger in winter than in summer. Yet, the impact of an aerosol layer on solar radiation depends on the SZA. For large SZA, the incidence angle over the aerosol layer is large and also is the time spend by solar beams on it (the optical path). The more time the beams spend on the aerosol layer, the more chance they have to be scattered or absorbed by aerosols and therefore, the more the photolysis rates are impacted.

3.3.2 Impact on 3-D concentrations

The vertical profiles of relative differences between R-AERO and R-COnL averaged over the spatial domain for O_3, NO_2, NO and OH concentrations are represented in Fig. 7 for July and November 2001. The largest differences are observed in OH and NO concentrations which are reduced all through the troposphere between 2 and 17% depending on altitude. These species are both directly produced by photolysis and they both have a short life-time. The changes in OH and NO concentrations are almost equivalent to changes in, respectively JO_1D and JNO_2 photolysis rates.

Differences in O_3 concentrations are mainly observed close to the ground. O_3 concentrations are impacted both by the decrease in JNO_2 (O_3 production) and the decrease in JO_1D (O_3 destruction). Therefore differences in O_3 concentrations are mostly observed where one of the two terms dominates. This is detailed in next section. NO_2 behaviour is complex. NO_2 concentrations increase at the ground both in November and July with R-AERO compared to R-COnL but they decrease just above the ground and up to 7 km in November. In July, they increase all through the troposphere except between 3 and 4 km height.

ACPD
10, 16691–16745, 2010

To understand the variations of NO_2 concentrations, the daily variations of JNO_2, NO, NO_2 and NO_3 (averaged over the month of November) are plotted at the ground and at 3 km (Fig. 8). The variations of the N_2O_5 concentrations are not shown but they are similar to the NO_3 ones (as a product of the reaction of NO_3 with NO_2) It can be seen that JNO_2 is reduced all through the day at the ground with R-AERO but with a larger decrease at the sun-set and sunrise due to larger SZA (and therefore larger optical path). At 3 km the same effect is observed but the presence of aerosol layers underneath leads to larger photolysis rates with R-AERO at noon and smaller decrease at sunrise and sun-set than at ground level. Furthermore, the chemistry which dominates NO_2 concentrations is different around noon and at night. During the day, and particularly around noon, NO_2 concentrations are mainly controlled by the NO_2 photolysis rate (for NO_2 loss) and by the reaction of NO with radicals or with O_3 (for NO_2 production). Therefore, at noon NO_2 concentrations changes will mainly follow changes in NO_2 photolysis rate. During the night, NO_2 is mainly destroyed through reactions with NO_3 and N_2O_5. In general, the attenuation of photolysis rates by aerosols induces an increase of NO_3 (NO_3 is less photolysed) and N_2O_5 concentrations at the beginning of the night leading to more NO_2 destruction. Overall this leads to different variations of NO_2 concentrations at the ground and at altitude as well as in summer and winter. Increasing altitude leads to lower decrease in JNO_2 photolysis rate (and even increase at noon in some cases) and then to less increase of daytime NO_2 concentrations. In summer, night is shorter and the increase in daytime NO_2 concentrations generally dominates nigh-time loss except around 3 km. In winter, the night-time loss dominates from 30 m to 7 km.

In term of tropospheric burden, NO and OH burdens both decrease by 10% in July and by, respectively 10 and 14% in November. The NO_2 tropospheric burden slightly increases in July (+2%) and decreases in November (−0.2%). O_3 tropospheric burden slightly decreases by around 2 and 1% in July and November, respectively, i.e. by around 2 $\mu g\,m^{-3}$.

ACPD
10, 16691–16745, 2010

The decrease in OH concentrations is also observed more generally in HO_x concentrations ($HO+HO_2$). Thus the oxidising capacity of the troposphere over Europe is globally reduced. This leads to a reduction of oxidation of several species and to an increase of their lifetime. This is the case for several VOCs as its is shown in the next section.

3.3.3 Impact on ground concentrations

In this section, the impact of solar radiation attenuation by aerosols on ground concentrations of gas but also aerosols is studied in details, and in particular the spatial heterogeneity of relative differences. Monthly maps are shown for July only.

Maps of ground relative differences between R-AERO and R-COnL for OH, O_3, NO_2 and NO are shown in Fig. 10. The map of OH relative differences is almost identical to the JNO_2 one (in fact it is linked to JO^1D, which varies similarly to JNO_2). The NO map is also similar to the JNO_2 one with noticeable differences over regions with strong NO_x emissions, i.e. urban regions where changes are small (see Fig. 9). In these regions, NO_x concentrations are dominated by emissions, the relative impact of photolysis being less important. However, it should be noticed that ,in contrast to the relative local differences, the absolute local differences in NO concentrations are larger over urban regions. As detailed in the previous paragraph, NO_2 concentrations increase over most of the domain. Concerning O_3, O_3 relative differences are important where one of the 2 terms: chemical O_3 production or destruction dominates. For example O_3 relative differences are larger around cities or in industrial valleys but also around ship emissions, with reductions up to 8% (see Fig. 9). In particular, O_3 peaks are reduced. Because O_3 has a relatively long life time and thus an elevated background, relative differences in rural regions (far from precursors emissions) are small compared to more reactive species such as OH or NO that have almost zero background concentrations. All these differences are enhanced in South Europe below dust plumes with mean relative differences in OH and NO around −30% and O_3 and NO_2 differences between −8 and +15%.

ACPD
10, 16691–16745, 2010

The map of relative differences in HNO_3 concentrations is also shown in Fig. 10. HNO_3 is formed by the reaction of NO_2 with OH. It can also be formed through the heterogeneous reaction of N_2O_5 (at night). Globally, HNO_3 concentrations decrease because of the decrease in OH concentrations that leads to a decrease in HNO_3 production during the day. NO_2 concentrations increase, increasing HNO_3 production, but to a lesser extent. During the night N_2O_5 concentrations increase (not shown, due to a decrease of NO_3 photolysis rates decrease) leading to an increase of night time HNO_3 production. Globally the decrease in HNO_3 production during the day dominates the increase in HNO_3 production during the night leading to a global reduction in HNO_3 concentrations except over two small areas in the Atlantic. Over these areas the NO_2 concentrations and therefore HNO_3 concentrations are small and clouds are important. The presence of clouds leads to a lower decrease of JO^1D than JNO_2, each photolysis rate being sensitive to different wavelengths which are scattered differently into clouds and aerosol layers. Therefore the decrease in OH is lower over these areas leading to a lower decrease in daily HNO_3 production. The increase in HNO_3 production at night becomes larger that its daily decrease explaining the mean increase in HNO_3 concentrations.

As explained in the previous section, the reduction of the oxidising capacity of the atmosphere is specially strong at the ground. This decrease impacts, in particular, the VOC lifetime, as reactions with OH are their main sources of chemical production or destruction. For example the ground concentrations of the model species HC_8 (aggregation of VOCs of 8 carbons) and isoprene are increased by, respectively 6 and 11% in July and 2 and 9% in November. The variations of isoprene are especially high because OH concentrations only influence the destruction of isoprene (in opposite to HC_8, isoprene is not formed through the oxidation of VOC by OH but directly emitted).

Not only gas, but also aerosol concentrations are impacted by the aerosol alteration of photolysis rates. Maps of monthly mean relative differences in PM_{10}, nitrate (PNO_3), sulphate (PSO_4), ammonium (PNH_4), and Secondary Organic Aerosols (PSOA) are represented in Fig. 11. PSO_4 concentrations mainly decrease over Europe due to the

ACPD
10, 16691–16745, 2010

decrease in OH concentrations (PSO_4 is produced by the condensation of H_2SO_4, a product of the oxidation of SO_2 by OH). Depending on the regions, PNO_3 concentrations can either increase or decrease when including the aerosol impact on solar radiation. PNO_3 is mostly formed by the condensation of HNO_3. Therefore, PNO_3 relative differences follow that of HNO_3 except when PSO_4 concentrations are high (over the Mediterranean sea and over North Africa for example). Over these regions, the absolute PSO_4 concentrations strongly decrease because of a decrease in OH and HNO_3 tends to condensate and replaces PSO_4 to neutralise PNH_4. PNH_4 is formed by the condensation of NH_3 onto particles depending on the concentrations of PNO_3 and PSO_4. Therefore changes in PNH_4 concentrations follow those of PNO_3 and PSO_4.

SOA concentrations mainly decrease. They are formed by the condensation of semi-volatile organic species (SVOC), which concentrations decrease mainly due to the decrease in OH concentrations, as they are produced through the oxidation of gas precursors (mainly by OH). When looking at SOA concentrations (see Fig. 9) it si clear that two different behaviours are simulated for anthropogenic and biogenic species (PAPI, PLIM). For biogenic, which are abundant over the Alps, around Biaritz and North Africa, relative differences are small, less than −1 or −2%, although differences around −10% are simulated for other SOA. This can be explain by the OH reactivity of the VOC gas precursors. Limonene (LIM) and alpha-pinene (API) which are the precursors for PLIM, and PAPI1, respectively, have higher OH reactivity than other anthropogenic VOC. The limiting factor to form SVOC is therefore not the concentrations of OH, but the concentrations of gas precursors

Overall, although higher differences are observed locally for PNO_3 and PSO_4 (up to −20% for PNO_3) they often compensate each other and the impact on PM_{10} is relatively small, with a maximum of −8% over the Po Valley.

3.3.4 Comparison with previous studies

Dickerson et al. (1997) first shown the importance of aerosols impact on photolysis rates and on photochemistry for case studies in 1-D (no horizontal dimension) The

ACPD
10, 16691–16745, 2010

first analyses of this impact over large regions were conducted from 2003 (Liao et al., 2003; Martin et al., 2003; Tie et al., 2005). These studies mainly focused on the impact on global tropospheric gas composition (O_3, NO_x and HO_x) and used global CTMs coupled to photolysis schemes to simulate this effect. The three studies mentioned above used a resolution of 4°×5°. To our knowledge, only one study was performed at a regional scale. Tang et al. (2003) simulated the aerosol impact on photolysis rates over Asia with a resolution of 80 km×80 km (approximately 5 times smaller than the global studies).

All these studies simulated a mean decrease of photolysis rates due to the impact of aerosols, with the largest decrease at the ground and sometimes an increase over regions with strongly scattering aerosols. However, photolysis rate reductions are different between studies. Liao et al. (2003) simulated a small impact of aerosols on photolysis rates whereas a large impact was simulated by Martin et al. (2003), especially in regions with strong dust loading (photolysis rate decrease of about 30% in North Africa) or strong BB emissions (decrease reaching 50% in India). Photolysis rate decreases simulated by Tie et al. (2005) were important but slightly smaller than Martin et al. (2003) (maximum over Africa with decrease around 40%). Impact of these photolysis rates modifications on gas concentrations (O_3, NO_x, OH) was evaluated to be important for global OH tropospheric burden but not really for global O_3 burden. However, strong regional impact was simulated (up to −5 to −15% of ground O_3 concentrations over BB regions). In the regional study of Tang et al. (2003), decreases were even stronger (up to −60% of ground photolysis rates over BB regions) leading to non negligible O_3 decreases (8%). O_3 decreases were also important in anthropogenic plume (Shangai), up to −15% of O_3 concentrations.

Over Europe, Martin et al. (2003) and Tie et al. (2005) simulated a decrease of ground JO^1D in summer ranging from −10 to −20% for Tie et al. (2005) and −30% for Martin et al. (2003). JNO_2 was slightly less impacted (from −5 to −25%). In both studies, the largest decrease was simulated in South Europe with dust influence but a high decrease was also simulated in North Europe (up to −25% in Martin et al., 2003)

ACPD
10, 16691–16745, 2010

mainly due to black carbon emissions. The same range of decrease in JO^1D and JNO_2 are simulated in this paper, ranging from 0 to 30%. However the strong reduction in North Europe is not simulated in our study because black carbon emissions are lower. Photolysis rates changes are also more spatially heterogeneous (because of the highest resolution) and the reductions over strong anthropogenic emission regions such as Paris or the Po Valley are more clear. In term of impact on gas concentrations, Tie et al. (2005) observed a decrease in OH concentrations that is slightly smaller than the decrease in JO_1D (from 0 to −10%) and O_3 changes from 1 to −2%. Martin et al. (2003) do not differentiate the impact of aerosols on gas due to the alteration of photolysis rates and due to heterogeneous reactions. impact on gas was not differentiated between photolysis rates alteration and heterogeneous reactions. However, authors estimated than in summer, the decrease of O_3 boundary layer concentrations by 5–9 ppbv in North Europe is mainly due to photolysis rate attenuation by aerosols. In our study, boundary layer OH concentrations decrease by around 14% and boundary layer O_3 between 0 and 8% (i.e. up to 6 ppbv) with a mean value of 3%. Impact on O_3 and OH is higher than in Tie et al. (2005). None of these previous studies analysed impact on VOC or aerosols and none of them estimated the impact on air quality monitoring and on threshold exceedances (see next section).

Differences between the studies may come from (1) the simulated aerosol concentrations, compositions and size distributions (which mainly depend on the aerosol emissions, the aerosol boundary conditions and the aerosol model) (2) the refractive indexes used for individual species (3) the way optical properties are computed (internal mixing, external mixing, core shell) (4) the photolysis scheme used.

Jeong and Sokolik (2007) showed that for the same mass concentrations of dust aerosols, photolysis rates are highly sensitive to size distribution and minearological composition (percentage of iron). This latter changes the refractive index of dust. Differences in calculated photolysis rates can be as high as 40% between two population of different size distribution and iron percentage. They also showed that for a mixture of dust and anthropogenic aerosols, the way optical properties are computed (internal

ACPD
10, 16691–16745, 2010

or external mixing, core shell) do not play a strong role unless black carbon fraction is very high. Tombette et al. (2008) also showed that differences in the aerosol model itself induce more changes on computed AOD than the different options that may be available when computing optical properties (e.g. assumptions of internal/external mixing, calculation of the wet index). In the studies previously mentioned (Tie et al., 2005; Martin et al., 2003; Liao et al., 2003; Tang et al., 2003), aerosol models were all different. In particular, all models assumed aerosols to be externally mixed, whereas the assumption of internal mixing is used in our study. Furthermore, different refractive index are used. Only Tang et al. (2003) used the complete OPAC refractive index as here. Two different photolysis schemes are also used (TUV or FAST-J). Therefore, it is difficult to estimate which parameter leads to the highest differences. If two studies use the same updated cross-sections, it is probable that errors from the aerosol distributions itself, i.e. aerosol emission, boundary conditions and aerosol model will lead to the highest incertitude followed by the refractive index used for each individual species.

3.4 Impact on air quality monitoring

3.4.1 Comparisons of ground model concentrations to observations

Model concentrations of O_3, NO_2 and PM_{10} at the ground are compared to the European ground base stations EMEP. Stations from the EMEP network are representative of "background" concentrations. The simulated AOD have also been compared with the OD measured from the AERONET network. The comparisons are done using the results of the 3 simulations: our reference simulation (R-ATT), the simulation with the on-line impact of clouds on photolysis rates (R-COnL) and the simulation with the on-line impact of both clouds and aerosols on photolysis rates (R-AERO).

For gas and aerosol concentrations (O_3, NO_2 and PM_{10}), comparisons are shown for the 3 simulations: R-ATT, R-COnL and R-AERO for the months of July and November in Tables 4–7. Statistics are not strongly influenced by the parametrisation used for

ACPD
10, 16691–16745, 2010

clouds (R-COnL versus R-ATT). Scores are slightly better with R-COnL with maximum differences in winter.

Statistics are slightly more influenced by the simulation of aerosol impact on photolysis rates but differences remain small. As shown in Table 3, NO_2, O_3 and PM_{10} are not the most impacted species and the small differences in EMEP statistics are not therefore surprising. The statistics that compare AOD with AERONET stations when dust are divided by 4 are rather good (see Table 2) giving some confidences on the impact of aerosols on photolysis rates. For hourly O_3, statistics are generally better when taking into account solar radiation attenuation by aerosols. For both months, the bias, the absolute error and the RMSE are reduced. Only correlation coefficients for July slightly decrease. Peaks O_3 are best reproduce in November but not in July. Differences between R-AERO and R-COnL are low for NO_2 and PM_{10}. The correlations are slightly higher with R-AERO. RMSE is the same for NO_2 and is slightly lower for PM_{10} in July and higher in November. NME and NMB slightly increase for NO_2 and PM_{10} in November and decrease for PM_{10} in July. It is difficult to conclude anything on these comparisons because different performances are simulated depending on species and seasons.

A sensitivity study was conducted by Roustan et al. (2010) with our model for the two months studied here. To evaluate the impact of a parametrisation, of a model input or of a numerical approximation, they compared a reference simulation to a simulation where one parameter is changed. To quantify the influence of the parametrisation, they compared both simulations at the ground in terms of NME, RMSE and NMB (statistics between the two simulations and not with any measurement). Then they rank the different simulations depending on their NME with the reference simulation. To evaluate the relative impact of taking into account R-AERO on O_3, NO_2, NO, OH and PM_{10} concentrations compared to other parametrisations of the model we have done a similar comparison between R-AERO and R-COnL for the same species and also for OH. Concerning daily O_3, NO_2 and SO_2, changes induced by taking into account solar radiation attenuation by aerosols rank at the 5th, 6th and 8th position, respectively

ACPD
10, 16691–16745, 2010

according to the ranking of Roustan et al. (2010). For O_3 and NO_2 ground concentrations, the impact of aerosols on photolysis rates is not as important as the impact of the vertical turbulent diffusion or the number of vertical layers. Boundary conditions are also important for O_3 and heterogeneous reactions for NO_2. If simulations are ranked following their bias instead of their RME, the simulation R-AERO exhibits the largest impact, just followed by the run where the vertical diffusion parametrisation is changed. In this latter, the bias is less systematic than in R-AERO. OH concentrations are also more impacted by R-AERO than by any other parametrisations tested in Roustan et al. (2010). R-AERO is also the second run that impact the most NO concentrations after the run where the vertical diffusion scheme is changed.

3.4.2 Impact on air quality thresholds

It was previously shown that taking into account aerosols when computing the photolysis rates at the ground leads to a slight decrease of the mean O_3 concentrations but also to a decrease in O_3 peaks. The decrease in O_3 peaks is stronger than the decrease in mean O_3 concentrations. Exceedance of the O_3 thresholds for O_3 peaks is the criterion used by authorities (e.g. in France) to inform the public about high pollution episode. If exceedances of the O_3 thresholds are to be obtained from numerical simulations rather than observations (for example for prevision), the impact of aerosols on photochemistry may be important. We calculate these thresholds over each model grid for R-COnL and R-AERO. Figure 12 shows the differences between R-COnL and R-AERO) in terms of number of exceedances of the O_3 information threshold (hourly concentrations>180 $\mu g\,m^{-3}$). About half of the O_3 exceedances are not simulated when taking solar radiation attenuation into account. Exceedances of the alert threshold (hourly concentrations>240 $\mu g\,m^{-3}$) are also divided by 2 (not shown). Those differences are particularly important because emissions of O_3 precursors and aerosols emissions are usually collocated. Therefore the AOD is particularly strong where O_3 production is the largest leading to strong O_3 peak reductions.

ACPD
10, 16691–16745, 2010

4 Conclusions

The impact of photolysis rate calculation on European air composition and air quality monitoring is studied. To do so, the photolysis scheme Fast-JX is used to (1) update the clear-sky photolysis rate tabulation used in the CTM POLAIR3D (2) more realistically simulate the cloud impact on photolysis rates by replacing the "attenuation coefficient" method by taking into account clouds directly in the computation of photolysis rates in Fast-JX (3) take into account the aerosol impact on photolysis rates by coupling FAST-JX and the CTM Polair3D. Two months are chosen to perform the simulations: July and November 2001.

The clear-sky tabulated rates calculated with FAST-JX exhibit large differences with the older one (calculated with the photolysis scheme J-PROC). Most photolysis rates show large increase (21 and 32% for JNO_2 and JO^1D, and up to 220% for HNO_4), mainly due to differences in cross-section data.

The more realistic parametrisation of clouds leads to differences in photolysis rates mainly inside clouds. In general, the highest the cloud optical depth is, the highest the differences are. Inside clouds, differences in the treatments of clouds for the computation of photolysis rates lead to differences of the same order of magnitude as differences between simulations with and without clouds (around 10%). Outside clouds, differences are small. The species the most impacted by the changes in photolysis rates are OH and NO because they are both directly produced by photolysis and have a small life-time. Inside clouds, local relative differences of OH concentrations are of the order of +5 to +11% in July and November, respectively. At the ground those differences are small. In terms of tropospheric burden, the largest impact is simulated for OH burden, which increases by 4 to 5%.

Taking into account the impact of aerosols on photolysis rates leads to stronger differences both in photolysis rates and concentrations. The higher impact on photolysis rates is observed at the ground and it decreases with altitude. At the ground, monthly mean photolysis rates are reduced by around 8% in summer and 16% in winter. Dust

ACPD
10, 16691–16745, 2010

is the aerosol species which impact the most photolysis rates. Its impact is particularly strong in South Europe as it is transported from North Africa. Strong impact is also observed over anthropogenic emission regions (Paris, The Po and the Ruhr Valley) where mainly PNO_3 and PSO_4 reduced the incoming radiation. Differences in photolysis rates lead to changes in species concentrations, with the largest impact simulated on OH and NO. Monthly mean ground concentrations of both species are reduced by around 10 to 14%. More generally, the tropospheric burden of OH and NO decreases by around 10%. The decrease in OH, strong oxidant species, leads to an increase in the life-time of several species and in particular several VOCs such as isoprene (10% increase). Tropospheric NO_2 concentrations are not strongly impacted, with relative differences equivalent to those obtained in the cloud parametrisation study (around 2%). O_3 concentrations mostly decrease at the ground with a monthly mean reduction of about 3%. But one of the strongest impact of solar radiation modification by aerosols is to systematically reduce strong O_3 peak values by reducing NO_2 photolysis rates. Not only gas concentrations are impacted by the solar radiation alteration by aerosols but also secondary aerosol concentrations. Monthly mean concentrations of PNO_3, PNH_4, PSO_4 and PSOA at the ground are modified by up to 4% but changes in aerosol species concentrations often compensate each other. This results in an increase in PM_{10} and $PM_{2.5}$ ground-burden of less than 1% in summer and around 2% in winter. However, local PM_{10} and $PM_{2.5}$ relative differences can reach decrease around 8% (in the Po valley).

In terms of air quality monitoring, ground O_3, NO_2 and PM_{10} concentrations simulated with the two cloud parametrisations and with aerosol impact on photolysis rates are compared with ground based measurement from the EMEP European network. Differences simulated on these species are small for cloud parametrisation and slightly higher for aerosol impact. Although scores are generally improved when taking into account aerosols when computing photolysis rates, differences are small. On the other hand, O_3 peaks are systematically reduced when including the impact of aerosols on photolysis rates. This results in large differences in exceedances of the European O_3

ACPD
10, 16691–16745, 2010

threshold as calculated by the model: the numbers of exceedances of the information and the alert threshold are divided by 2.

Acknowledgements. We thank Oliver Wild and Michael J. Prather for use of the Fast-JX model. We are also gratful to Michael Mishchenko for providing the Mie code use in this paper and to Maryline Tombette for useful informations on optical properties calculation.

References

Barnard, J. C., Chapman, E. G., Fast, J. D., Schmelzer, J. R., Slusser, J. R., and Shetter, R. E.: An evaluation of the FAST-J photolysis algorithm for predicting nitrogen dioxide photolysis rates under clear and cloudy sky conditions, Atmos. Environ., 38, 3393–3403, 2004. 16698

Briegleb, B. P.: Delta-eddington approximation for solar radiation in the NCAR community climate model, J. Geophys. Res., 97, 7603–7612, 1992. 16700

Carmichael, G., Sakurai, T., Streets, D., Hozumi, Y., Ueda, H., Park, S., Fung, C., Han, Z., Kajino, M., Engardt, M., Bennet, C., Hayami, H., Sartelet, K., Holloway, T., Wang, Z., Kannari, A., Fu, J., Matsuda, K., Thongboonchoo, N., and Amann, M.: MICS-Asia II: The model intercomparison study for Asia Phase II methodology and overview of findings, Atmos. Environ., 42, 3468–3490, 2008. 16696

Chang, J., Brost, R., Isaken, I., Madronich, S., Middleton, P., Stockwell, W., and Walcek, C.: A three-dimensional Eulerian acid deposition model: physical concepts and formulation, J. Geophys. Res., 102, 14681–14700, 1987. 16698, 16705, 16727

Chin, M., Rood, R., Lin, S.-J., Muller, J., and Thomspon, A.: Atmospheric sulfur cycle in the global model GOCART: model description and global properties, J. Geophys. Res., 105, 24671–24687, 2000. 16701

Collins, W. D.: Parameterization of generalized cloud overlap for radiative calculations in general circulation models, J. Atmos. Sci., 58, 3224–3242, 2001. 16700

Debry, E., Fahey, K., Sartelet, K., Sportisse, B., and Tombette, M.: Technical Note: A new SIze REsolved Aerosol Model (SIREAM), Atmos. Chem. Phys., 7, 1537–1547, doi:10.5194/acp-7-1537-2007, 2007. 16696

Demerjian, K. L., Schere, K., and Peterson, J.: Theoretical estimates of actinic (spherically integrated) flux and photolytic rate constants of atmospheric species in the lower troposphere, Adv. Environ. Sci. Technol., 10, 369–459, 1980. 16727

ACPD

10, 16691–16745, 2010

DeMore, W. B., Sander, S., Golden, D., Hampson, R., Kurylo, M., Howard, C., Ravishankara, A., Kolb, C., and Molina, M.: Chemical Kinetics and Photochemical Data for Use in Stratospheric Modeling: Evaluation Number 11, Tech. rep., 1994. 16727

Dickerson, R. R., Kondragunta, S., Stenchikov, G., Civerolo, K. L., Doddridge, B. G., and Holben, B. N.: The impact of aerosols on solar ultraviolet radiation and photochemical smog, Science, 278, 827–830, 1997. 16714

Elterman, L.: UV, Visible, and IR Attenuation for Altitudes to 50 km, Air Force Cambridge Res. Lab., AFCRL-68-0153, Tech. rep., Bedford, MA, 1968. 16727

Fahey, K. and Pandis, S.: Size-resolved aqueous-phase chemistry in a three-dimensional chemical transport model, J. Geophys. Res., 108, 4690, doi:10.1029/2003JD003564, 2003. 16697

Feng, Y., Penner, J. E., Sillman, S., and Liu, X.: Effects of cloud overlap in photochemical models, J. Geophys. Res., 109, D04310, doi:10.1029/2003JD004040, 2004. 16700

Geleyn, J. F. and Hollingsworth, A.: An economical analytical method for the computation of the interaction between scattering and line absorption of radiation, Cont. Atmos. Physics, 52, 1–16, 1992. 16700

Gery, M., Whitten, G., Killus, J., and Dodge, M.: A photochemical mechanism for urban and regional scale computer modeling, J. Geophys. Res., 94, 12925–12956, 1989. 16727

He, S. and Carmichael, G. R.: Sensitivity of photolysis rates and ozone production in the troposphere to aerosol properties, J. Geophys. Res., 104, 26307–26324, 1999. 16709

Hess, M., Koepke, P., and Schult, I.: Optical properties of aerosols and clouds: the software package OPAC, B. Am. Meteorol. Soc., 79, 831–845, 1998. 16701

Horowitz, L., Walters, S., Mauzerall, D., Emmons, L., Rasch, P., Granier, C., Tie, X., Lamarque, J.-F., Schultz, M., Tyndall, G., Orlando, J., and Brasseur, G.: A global simulation of tropospheric ozone and related tracers: Description and evaluation of MOZART, version 2, J. Geophys. Res., 108, 4784, doi:10.1029/2002JD002853, 2003. 16701

Jeong, G.-R. and Sokolik, I. N.: Effect of mineral dust aerosols on the photolysis rates in the clean and polluted marine environments, J. Geophys. Res., 112, 387–422, 2007. 16716

Joseph, J., Wiscombe, W., and Weinman, J.: The delta-Eddington approximation for radiative flux transfer, J. Atmos. Sci., 33, 2452–2459, 1976. 16697

Krysta, M., Bocquet, M., Sportisse, B., and Isnard, O.: Data assimilation for short-range dispersion of radionuclides: an application to wind tunnel data, Atmos. Environ., 40, 7267–7279, 2006. 16696

ACPD
10, 16691–16745, 2010

Labow, G. J., McPeters, R. D., and Bhartia, P. K.: A comparison of TOMS and SBUV version 8 total column ozone data with data from ground stations, Proceedings of the XX Quadrennial Ozone Symposium, edited by: Zerefos, C. S., Int. Ozone Comm., Athen, 123–124, 2004. 16727

Liao, H., Adams, P. J., Chung, S. H., Seinfeld, J. H., Mickley, L. J., and Jacob, D. J.: Interactions between tropospheric chemistry and aerosols in a unified general circulation model, J. Geophys. Res., 108, 4001, doi:10.1029/2001JD001260, 2003. 16695, 16715, 16717

Mallet, V.: Estimation de l'incertitude et prevision d'ensemble avec un modèle de chimie-transport, Tech. rep., These de doctorat de l'ENPC, 2005. 16696, 16698

Martin, R. V., Jacob, D. J., Yantosca, R. M., Chin, M., and Ginoux, P.: Global and regional decreases in tropospheric oxidants from photochemical effects of aerosols, J. Geophys. Res., 108, 4097, doi:10.1029/2002JD002622, 2003. 16695, 16715, 16716, 16717

Mishchenko, M. I., Goegdzhayev, I., Cairns, B., Rossow, W. B., and Lacis, A. A.: Aerosol retrievals over the ocean by use of channels 1 and 2 AVHRR data: sensitivity analysis and preliminary results, Appl. Optics, 38, 7325–7341, 1999. 16701

Nenes, A., Pandis, S. N., and Christodoulos, P.: ISORROPIA: a new thermodynamic equilibrium model for multiphase multicomponent inorganic aerosols, Aquat. Geochem., 4, 123–152, 1998. 16697

Neu, J. L., Prather, M. J., and Penner, J. E.: Global atmospheric chemistry: integrating over fractional cloud cover, J. Geophys. Res., 112, D11306, doi:10.1029/2006JD008007, 2007. 16700

Pozzoli, L., Bey, I., Rast, S., Schultz, M. G., Stier, P., and Feichter, J.: Trace gas and aerosol interactions in the fully coupled model of aerosol-chemistry-climate ECHAM5-HAMMOZ: 1. Model description and insights from the spring 2001 TRACE-P experiment, J. Geophys. Res., 113, D07308, doi:10.1029/2007JD009007, 2008. 16699, 16700

Rockel, B., Raschke, E., and Weyres, B.: A parametrization of broad band radiative transfer properties of water, ice and mixed clouds, Beitr. Phys. Atmos., 64, 1–12, 1991. 16699

Roustan, Y. and Bocquet, M.: Sensitivity analyse for mercury over Europe, J. Geophys. Res., 111, D14304, doi:10.1029/2005JD006616, 2006. 16696

Roustan, Y., Sartelet, K. N., Tombette, M., Debry, E., and Sportisse, B.: Simulation of aerosols and gas-phase species over Europe with the Polyphemus system, Part II: model sensitivity analysis for 2001, Atmos. Environ., under review, 2010. 16718, 16719

ACPD
10, 16691–16745, 2010

Sander, S., Friedl, R. R., Ravishankara, A. R., Golden, D. M., Kolb, C. E., Kurylo, M. J., Molina, M. J., Huie, R. E., Orkin, V. L., Moortgat, G. K., and Finlayson-Pitts, B. J.: Chemical Kinetics and Photochemical Data for Atmospheric Studies, JPL Pub. 02-25, Jet Propulsion Lab, Pasadena, CA, 2003, 2002. 16703, 16727

Sartelet, K., Debry, E., Fahley, K., Roustan, Y., Tombette, M., and Sportisse, B.: Simulation of aerosols and gas-phase species over Europe with the Polyphemus system: Part I: Model-to-data comparison for 2001, Atmos. Environ., 41, 6116–6131, 2007a. 16696, 16701, 16702

Sartelet, K. N., Hayami, H., and Sportisse, B.: Dominant aerosol processes during high-pollution episodes over Greater Tokyo, J. Geophys. Res., 112, D14214, doi:10.1029/2006JD007885, 2007b. 16696

Schell, B., Ackermann, I., Hass, H., Binkowski, F., and Ebel, A.: Modeling the formation of secondary organic aerosol within a comprehensive air quality model system, J. Geophys. Res., 106, 28275–28293, 2001. 16697

Stockwell, W. R., Kirchner, F., and M. Kuhn, S. S.: A new mechanism for regional atmospheric chemistry modelling, J. Geophys. Res., 102, 25847–25879, 1997. 16696

Tang, Y., Charmichael, G. R., Woo, J.-H., Thongboonchoo, N., Kurata, G., Uno, I., Streets, D. G., Blake, D. R., Weber, R. J., Talbot, R. W., Kondo, Y., Singh, H. B., and Wang, T.: Influences of biomass burning during the Transport and Chemical Evolution Over the Pacific (TRACE-P) experiment identified by the regional chemical transport model, J. Geophys. Res., 108(D21), 8824, doi:10.1029/2002JD003110, 2003. 16695, 16715, 16717

Tie, X., Madronich, S., Walters, S., Edwards, D. P., Ginoux, P., Mahowald, N., Zhang, R., Lou, C., and Brasseur, G.: Assessment of the global impact of aerosols on tropospheric oxidants, J. Geophys. Res., 110, D03204, doi:10.1029/2004JD005359, 2005. 16695, 16715, 16716, 16717

Tombette, M., Chazette, P., Sportisse, B., and Roustan, Y.: Simulation of aerosol optical properties over Europe with a 3-D size-resolved aerosol model: comparisons with AERONET data, Atmos. Chem. Phys., 8, 7115–7132, doi:10.5194/acp-8-7115-2008, 2008. 16701, 16717

Vautard, R., Bessagnet, B., Chin, M., and Menu, L.: On the contribution of natural aeolian sources to particulate matter concentrations in Europe: testing hypotheses with a modelling approach, Atmos. Environ., 39, 3291–3303, 2005. 16701

Voulgarakis, A., Savage, N. H., Wild, O., Carver, G. D., Clemitshaw, K. C., and Pyle, J. A.: Upgrading photolysis in the p-TOMCAT CTM: model evaluation and assessment of the role of clouds, Geosci. Model Dev., 2, 59–72, doi:10.5194/gmd-2-59-2009, 2009. 16698

ACPD
10, 16691–16745, 2010

Wang, P.-H., McCormick, M. P., Chu, W. P., Lenoble, J., Nagatani, R. M., Chanin, M. L., Barnes, R. A., Schmidlin, F., and Rowland, M.: SAGE II Stratospheric Density and Temperature Retrieval Experiment, J. Geophys. Res., 97, 843–863, 1992. 16727

Wang, J. H. and Rossow, W. B.: Effects of cloud vertical structure on atmospheric circulation in the GISS GCM, J. Climate, 11, 3010–3029, 1998. 16700

Wild, O. and Akimoto, H.: Intercontinental transport of ozone and its precursors in a three-dimensional global CTM, J. Geophys. Res., 106, 27729–27744, 2001. 16697, 16703

Wild, O., Zhu, X., and Prather, M. J.: Fast-J: accurate simulation of in- and below-cloud photolysis in tropopsheric chemical models, J. Atmos. Chem., 37, 245–282, 2000. 16699, 16705, 16708

ACPD

10, 16691–16745, 2010

Table 1. Model schemes, characteristics and parameters.

	Scattering treatment	Number of wavelength bins	O_3 vertical profile	Temperature profile	aerosol profile	O2 profile	Earth albedo	Cross section
J-PROC	2-stream	170	DeMore et al. (1994)	Chang et al. (1987)	Elterman (1968) OD at 340 nm: 0.379	DeMore et al. (1994)	Demerjian et al. (1980)	Gery et al. (1989) and JPL 94 (DeMore et al., 1994)
FAST-JX	multiple scattering (8 stream)	18	Labow et al. (2004)	Wang et al. (1992)	NONE	IDEM	0.1	Mainly JPL 02 (Sander et al., 2002)

ACPD
10, 16691–16745, 2010

Table 2. Statistics obtained when comparing model OD calculated with boundary conditions from GOCART dust concentrations (standard) and the same concentrations divided by 4 (Dust/4), with AERONET OD data. Mean values and RMSE are reported in $\mu g\,m^{-3}$, and RMSE, NMB and NME in %.

	Summer					Winter				
	mean	*r*	RMSE	NMB	NME	mean	*r*	RMSE	NMB	NME
Measurements	0.2					0.2				
Standard	0.6	73.9%	0.5	128%	137%	0.3	47.7%	0.3	117%	122%
Dust/4	0.3	78.1%	0.2	20%	43%	0.2	57.4%	0.1	44%	57%

ACPD
10, 16691–16745, 2010

Table 3. Monthly relative differences between R-AERO and R-COnL in tropospheric burden for July and November.

Species	O_3	NO_2	NO	OH	ISO	HC_8	PM_{10}	$PM_{2.5}$	PNO_3	PSO_4	PNH_4	SOA
Summer – tropospheric	−2%	+2%	−10%	−10%	+11%	+6%	−0.1%	−0.5%	+0.7%	−2%	+1%	−1%
Summer – ground	−3%	+2%	−13%	−14%	+8%	+5%	−0.2%	−0.7%	+0.7%	−3%	−1%	−2%
Winter – tropospheric	−0.8%	−0.2%	−14%	−10%	+9%	+2%	+2%	+2%	+4%	+1%	+3%	−1.4%
Winter – ground	−2.5%	−0.6%	−13%	−13%	+8%	+2%	+2%	+2%	+3%	+0.3%	+3%	−2%

ACPD
10, 16691–16745, 2010

Table 4. Statistics obtained when comparing hourly O_3 measured and simulated at EMEP stations with R-Att, R-COnL and R-AERO in July and November. Mean values and RMSE are reported in $\mu g\,m^{-3}$, and RMSE, NMB and NME in %.

	Summer					Winter				
	mean	*r*	RMSE	NMB	NME	mean	*r*	RMSE	NMB	NME
Measurements	74.7					39.8				
R-Att	84.5	54.3%	28.0	18%	33.2%	44.9	43.7%	19.8	19%	44.2%
R-COnL	84.6	54.4%	28.1	19%	33.4%	44.9	44.3%	19.7	18%	44%
R-AERO	81.9	53.9%	27.5	15%	32.1%	43.4	45.7%	19.2	14%	42.4%

ACPD
10, 16691–16745, 2010

Table 5. Same caption as in Table 4 but for O_3 daily peaks.

	Summer mean	r	RMSE	NMB	NME	Winter mean	r	RMSE	NMB	NME
Measurements	99.1					51				
R-Att	97.4	60.1%	23.3	+1%	19.7%	54.7	37%	17.7	9%	29.1%
R-COnL	98.6	60.2%	23.3	+2%	19.7%	54.6	38.3%	17.4	9%	28.7%
R-AERO	95.5	59.5%	23.7	−1%	19.8%	52.8	40.9%	16.9	5%	27.6%

ACPD
10, 16691–16745, 2010

Table 6. Same caption as in Table 4 but for daily NO_2 concentrations.

	Summer mean	*r*	RMSE	NMB	NME	Winter mean	*r*	RMSE	NMB	NME
Measurements	4.8					10.3				
R-Att	4.2	32.3%	2.5	13%	63.7%	10.2	32.8%	6.4	52%	93.4%
R-COnL	4.1	32.3%	2.5	10%	62.7%	10.2	32.7%	6.4	52%	93.6%
R-AERO	4.2	32.9%	2.5	13%	63.9%	10.4	33.2%	6.4	54%	94.6%

ACPD
10, 16691–16745, 2010

Table 7. Same caption as in Table 4 but for daily PM_{10} concentrations.

	Summer mean	*r*	RMSE	NMB	NME	Winter mean	*r*	RMSE	NMB	NME
Measurements	18.7					16.2				
R-Att	10.9	71.4%	9.9	–37%	42.1%	14.3	44.4%	10.2	62.6%	17%
R-COnL	10.9	71.5%	9.9	–37%	42.1%	14.3	44.4%	10.2	62.6%	17%
R-AERO	10.9	72.1%	9.8	–36%	42%	14.6	44.7%	10.3	64.6%	21%

ACPD
10, 16691–16745, 2010

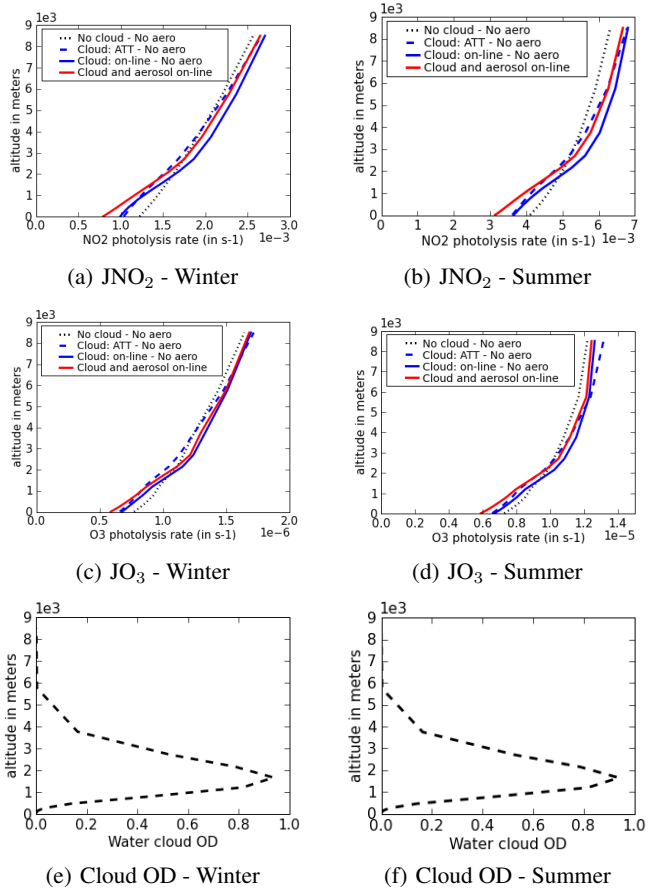

(a) JNO_2 - Winter (b) JNO_2 - Summer

(c) JO_3 - Winter (d) JO_3 - Summer

(e) Cloud OD - Winter (f) Cloud OD - Summer

Fig. 1. Mean vertical profiles of JNO_2 and JO_3 calculated for clear sky conditions, with R-Att, with R-COnL and with R-AERO for July and November 2001. Calculated cloud OD are also shown for the 2 months.

ACPD
10, 16691–16745, 2010

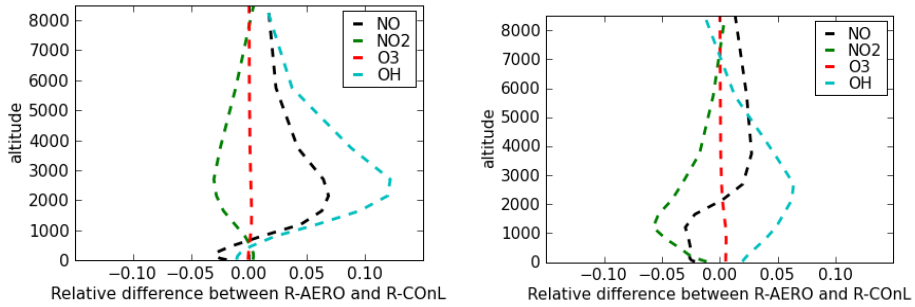

(a) November (b) July

Fig. 2. Relative differences between O_3, NO, NO_2 and OH concentrations simulated using the "attenuation" and the "on-line" cloud parametrisations. Values are averaged over Europe and over November (left panel) and July 2001 (rigth panel).

ACPD
10, 16691–16745, 2010

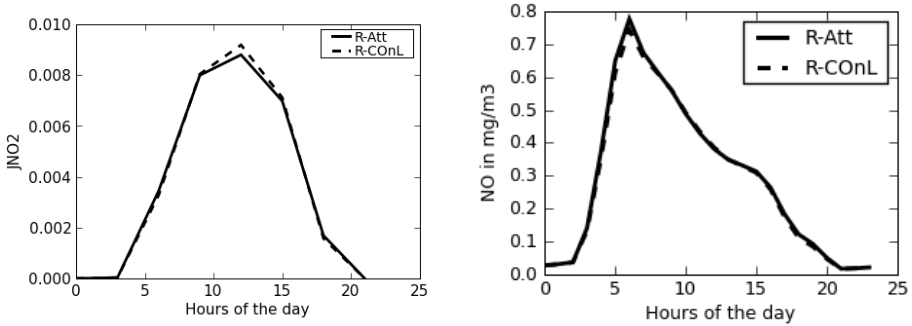

(a) JNO_2 (b) NO

Fig. 3. Monthly mean daily variations of JNO_2 and NO concentrations in July for the simulations R-ATT and R-COnL.

ACPD
10, 16691–16745, 2010

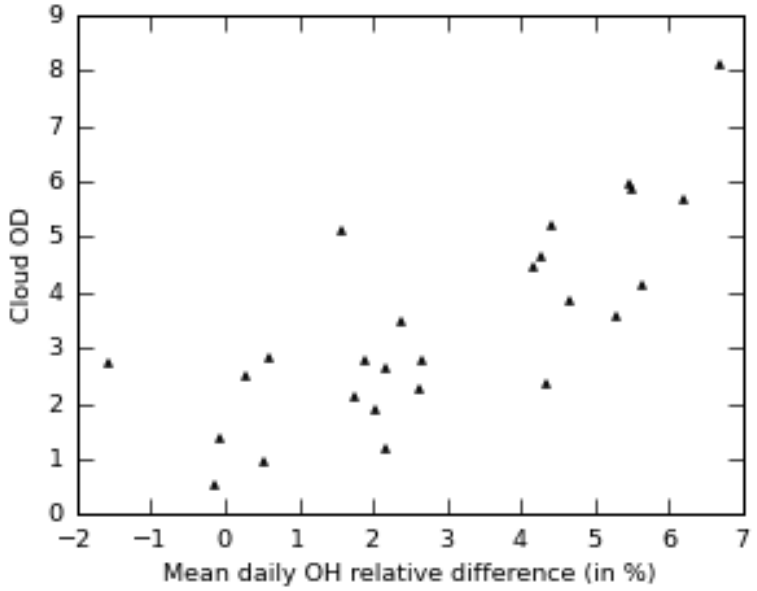

Fig. 4. Daily mean cloud OD versus OH relative differences between R-ATT and R-COnL at the ground. Relative differences are averaged over the spatial domain and represented for each day of July.

ACPD
10, 16691–16745, 2010

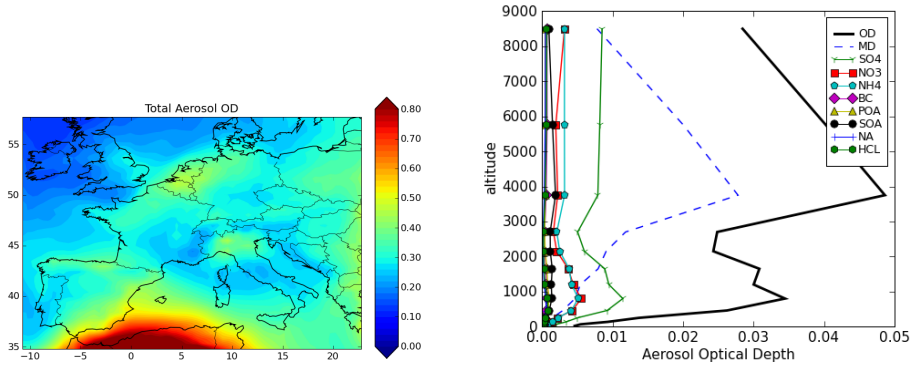

(a) Map (b) Vertical profile

Fig. 5. (a) Monthly mean tropospheric AOD and **(b)** vertical profile for July 2001. The contributions of individual aerosol species to OD are also shown in the vertical profile.

ACPD
10, 16691–16745, 2010

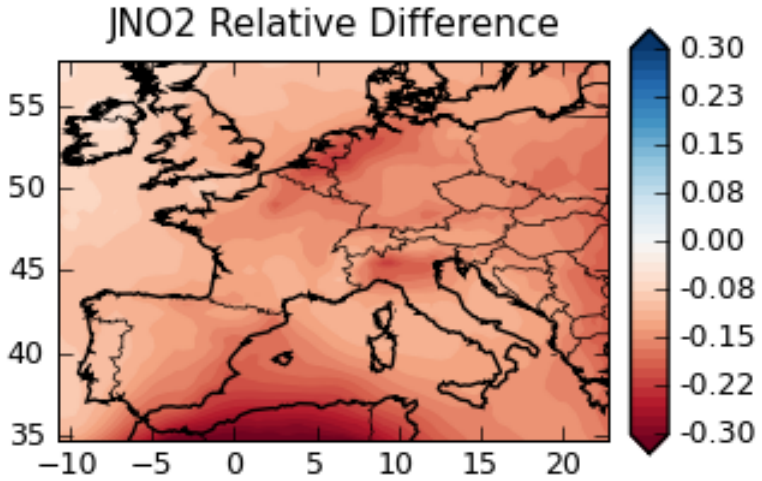

Fig. 6. Monthly mean relative difference in JNO_2 between R-AERO and R-COnL for July 2001.

ACPD
10, 16691–16745, 2010

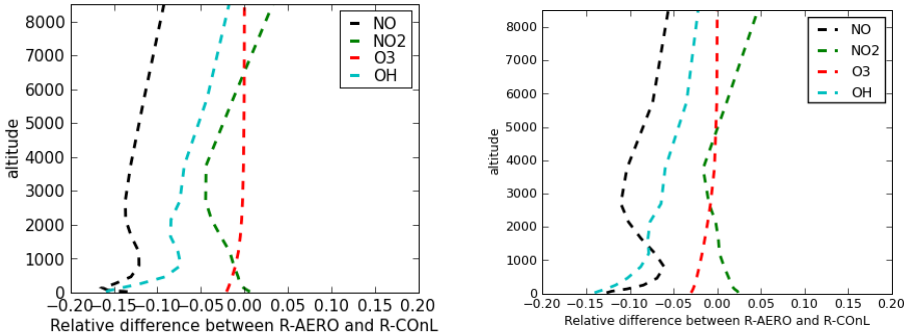

(a) November (b) July

Fig. 7. Relative differences between O_3, NO, NO_2 and OH concentrations simulated with and without aerosol impact on photolysis rates. Values are averaged over Europe for November (left panel) and July 2001 (right panel).

ACPD
10, 16691–16745, 2010

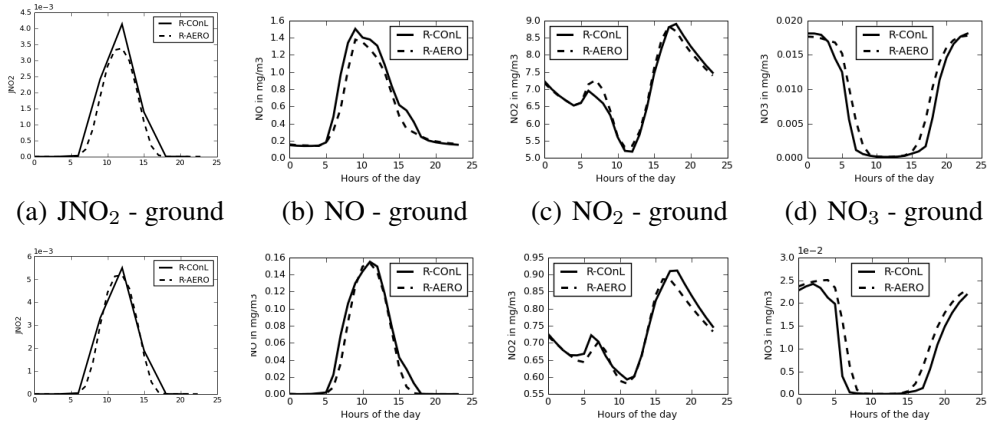

(a) JNO_2 - ground (b) NO - ground (c) NO_2 - ground (d) NO_3 - ground

(e) JNO_2 - 3 km (f) NO - 3 km (g) NO_2 - 3 km (h) NO_3 - 3 km

Fig. 8. Monthly mean daily variations of JNO_2, NO, NO_2, and NO_3 concentrations at the ground and at 3 km, for the simulations R-AERO and R-COnL in November.

ACPD
10, 16691–16745, 2010

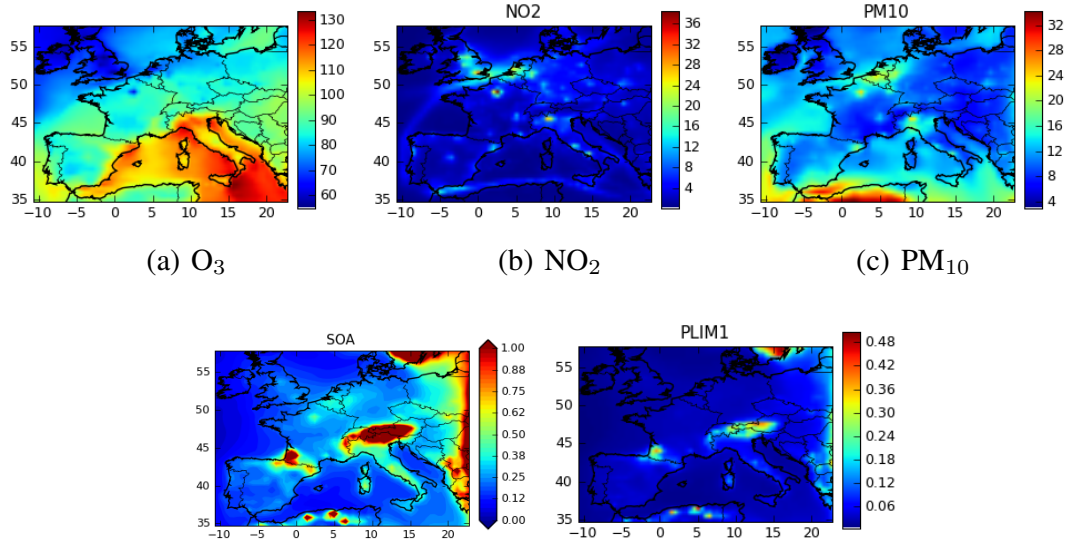

(a) O_3 (b) NO_2 (c) PM_{10}

(d) SOA (e) LIM

Fig. 9. Monthly mean concentrations of O_3, NO_2, PM_{10}, SOA and limonene at the ground for July 2001.

ACPD
10, 16691–16745, 2010

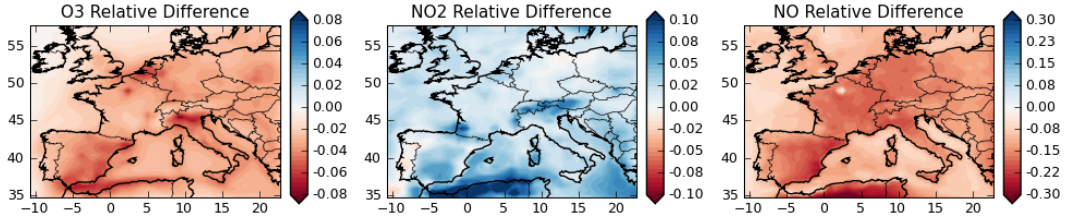

(a) O_3 (b) NO_2 (c) NO

(d) OH (e) HNO_3

Fig. 10. Monthly mean relative differences of NO_2, NO, O_3, OH and HNO_3 concentrations at the ground between the simulations R-AERO and R-COnL for July 2001.

ACPD
10, 16691–16745, 2010

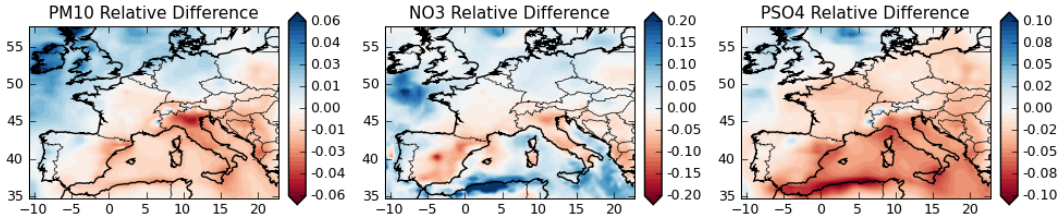

(a) PM_{10} (b) PNO_3 (c) SO4

(d) NH_4 (e) SOA

Fig. 11. Monthly mean relative differences of PM_{10}, PNO_3, PSO_4, PNH_4 and PSOA concentrations at the ground between the simulations R-AERO and R-COnL for July 2001.

ACPD
10, 16691–16745, 2010

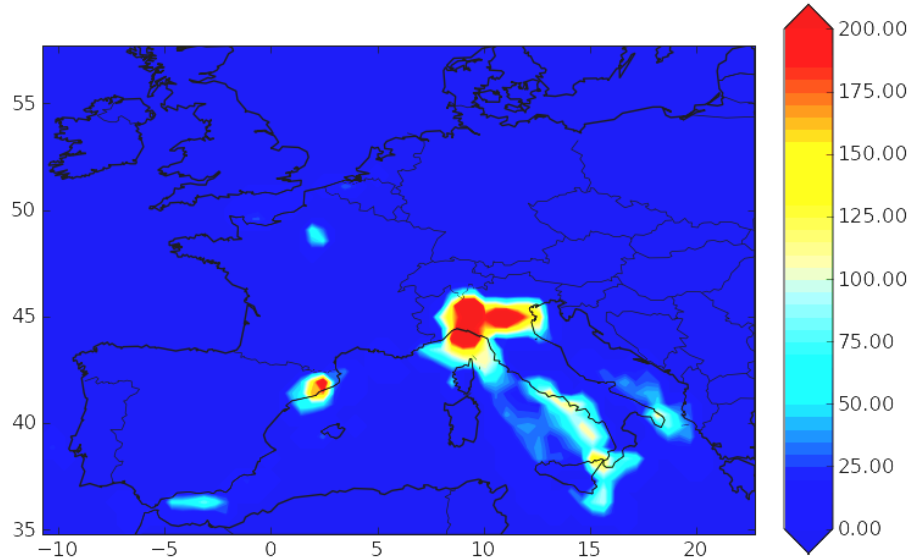

Fig. 12. Differences in number of exceedances of the European O_3 information threshold between R-COnL and R-AERO.

ACPD
10, 16691–16745, 2010